International Journal of Heat and Technology
Vol. 41, No. 5, October, 2023, pp. 1129-1138
Journal homepage: http://iieta.org/journals/ijht

Effect of Nanoparticle Material, Porosity and Thermal Radiation on Forced Convection Heat Transfer of Cu-Water and CuO-Water Nanofluids over a Stretching Sheet

Issam Rezaiguia[1*], Ridha Mebrouk[1], Mahfoud Kadja[2]

[1] Faculty of Hydrocarbons, Renewable Energy and Earth and Universe Science, Kasdi Merbah University, Ouargla 30000, Algeria
[2] Faculty of Technology Sciences, Department of Mechanical Engineering, Brothers Mentouri University – Constantine 1, Constantine 25000, Algeria

Corresponding Author Email: rezaiguiaissam@univ-ouargla.dz

https://doi.org/10.18280/ijht.410503

Received: 23 February 2023
Revised: 18 July 2023
Accepted: 14 August 2023
Available online: 31 October 2023

Keywords:
stretching sheet, nanofluid, forced convection, porous medium, nanofluid heat transfer, numerical simulation, magnetohydrodynamics

ABSTRACT

This study presents an examination of the incompressible magneto-hydrodynamic flow of water-based nanofluids, specifically Cu-water and CuO-water, over a stretching sheet within a porous medium under the influence of a magnetic field and radiation. The primary objective is to discern the effects of the nanoparticle volume fraction, magnetic field strength, Darcy number, Reynolds number, suction parameter, and radiation conductivity parameter on the heat transfer and friction characteristics of the nanofluid flow. The governing flow equations, initially in the form of partial differential equations, were transformed into nonlinear ordinary differential equations via the application of similarity variables. The resulting boundary value problem was tackled numerically utilizing the fourth-order Runge-Kutta method coupled with the shooting technique. The findings revealed velocity and temperature profiles, the coefficient of local friction, and the Nusselt number as functions of the controlling parameters for both types of nanofluids. It was observed that enhancements in the Darcy number, magnetic field strength, Reynolds number, and suction parameter corresponded to a decline n nanofluid velocity. Conversely, a rise in the nanoparticle volume fraction, magnetic field strength, and radiation parameter was associated with an increase in temperature profile, with the opposite effect noted for the Darcy number, Reynolds number, and suction parameter. Notably, CuO nanoparticles exhibited superior heat transfer performance. These insights potentially pave the way for optimized nanoparticle selection and porosity management in nanofluids, thereby advancing heat transfer enhancement and skin friction reduction in the presence of magnetic fields and thermal radiation.

1. INTRODUCTION

Over the past few decades, fluid flow through a stretching sheet has garnered significant attention due to its wide-ranging industrial applications, including hot metal rolling, wire drawing, glass-fiber production, paper production, drawing of plastic films, and metal and polymer extrusion processes. In these contexts, the rate of heat transfer is crucial, as cooling substantially influences the quality of the end product, which must meet specific requirements [1]. Consequently, research in this area has been oriented towards enhancing the thermal properties of fluids to increase the heat transfer rate between the fluid and the stretching surface.

Historically, studies on heat transfer have utilized fluids with low thermal conductivity, restricting heat transfer rates. To overcome this limitation, Das et al. [2] first pioneered techniques to augment heat exchange coefficients, which involved the addition of solid particles with high thermal conductivity to the liquid to be improved. These novel fluids were termed "nanofluids" due to the inclusion of nanoscale particles (usually smaller than 100 nm) in the liquid composition. The advent of nanofluids in the last thirty years has enabled the design of cost-effective equipment that enhances heat transfer without necessitating complex and expensive engineering solutions such as fins and obstacles [3]. Numerous studies have explored the use of nanofluids in various geometries like shell, rotating channel, and surfaces under different effects such as magnetic, thermal radiation, and viscoelastic effects, with or without the presence of a porous medium. For instance, Balla et al. [4] used the finite element method to investigate the natural convection nanofluid flow inside an inclined porous square cavity with four different nanoparticles in the presence of a magnetic field. They concluded that heat transfer enhances with the increase of the inclination angle, reaching a maximum at θ=45°. Abdollahi et al. [5] numerically investigated the effect of four different metal nanoparticles (SiO_2, Al_2O_3, CuO, and ZnO) in a square microchannel with imposed constant wall heat flux and longitudinal inner fins. They found that the increase of nanoparticle volume fraction with longitudinal fins enhances the performance of the microchannel. Aghaei et al. [6] numerically studied forced convection nanofluid flow in turbulent tube flows and concluded that with increasing Reynolds numbers, the Nusselt number values increase, the pressure drop increases, and the skin friction factor decreases for all considered volume fractions. The review by Gundabattini et al. [7] underlined the importance of using nanofluids to enhance thermal energy transfer, particularly in

cooling systems for electric machines, heat pipes, cryogenic cooling, and electronic devices. Devices like solar cells, microprocessors, and batteries generate considerable waste heat during operation, which if not properly dissipated, can reduce device efficiency, reliability, and lifespan, or even result in catastrophic failures. Ho et al. [8] experimentally studied the effect of adding nanometals (alumina) to a base fluid (water) in a heated tube with constant wall heat flux and found that metallic nanoparticles improve heat transfer acceleration, thus enhancing cooling performance. Zubair et al. [9] experimentally investigated nanofluid flow in engine radiator tubes using an ethylene glycol-based TiO_2 nanocooler, and demonstrated that a small concentration of nanoparticles and a high volumetric flow rate can enhance the heat transfer coefficient of the nanocooler, thereby increasing the maximum heat transfer enhancement.

In recent times, the impact of radiation on the hydromagnetic boundary layer flow of a stretching surface has been a subject of considerable scrutiny, driven by its numerous industrial applications. The seminal work by Crane [10], who was the first to examine the boundary layer flow instigated by a stretching sheet with a linearly varying velocity from a fixed point, spurred further investigation into this field. Subsequently, Carragher and Crane [11] delved into the heat transfer aspect of the problem, investigating a scenario wherein the temperature difference between the surface and the ambient fluid was proportional to the power of the distance from a fixed point. Further extending this line of inquiry, Magyari and Keller [12] analyzed the steady boundary layer flow on a stretching surface exhibiting an exponential temperature distribution. Sajid and Hayat [13] then explored the influence of thermal radiation on the flow over an exponential stretching sheet, employing the homotopy analysis method to provide an analytical solution to the problem.

In parallel with these investigations, a considerable number of studies have been undertaken over the last few decades into boundary layer flow over a stretching sheet in a magnetic field or a porous medium. In one notable study, Ramya et al. [14] contemplated the steady two-dimensional MHD flow of a viscous nanofluid over a non-linear stretching sheet, culminating in an analysis of both flow and heat transfer characteristics for the boundary layer. Similarly, Ahmed and Pop [15] examined the steady mixed convection boundary layer flow past a vertical flat plate embedded in a porous medium filled with nanofluids.

Despite these extensive investigations, a research gap persists regarding the influence of nanoparticle material, porous matrix, and radiation on MHD flow and heat transfer of nanofluids over stretching sheets. Consequently, the objective of this paper is to numerically investigate these effects. The governing equations were transformed into non-linear ODEs and subsequently solved using the RK4 method with the shooting technique. The analysis focuses on the effects of the governing parameters on velocity, temperature, skin friction, and Nusselt number, with the results discussed in detail.

2. FORMULATION OF THE PROBLEM

The flow investigated is steady, incompressible, two-dimensional and takes place in a Darcian porous medium of permeability K_p, over a perforated stretching sheet, with velocity u_w. The flowing fluid is an electrically conducting nanofluid. A magnetic field having a uniform strength B_0 is applied normally to the sheet. As a result of the stretching, a boundary layer forms above the sheet surface. Suction is applied to this boundary layer and takes place with a constant velocity v_w. This is used to prevent boundary layer separation. The transport properties of the fluid are assumed to be independent of temperature. We also assumed that the induced magnetic field is negligible. The sheet stretches along the x-axis. The y-axis is taken to be normal to the sheet while the coordinates origin remains fixed at x=0 and y=0. The flow configuration, the boundary conditions and the coordinate system are shown in Figure 1. Under the above assumptions and boundary layer approximations, the equations governing the problem can be written in dimensional form as:

$$\frac{\partial u}{\partial x}+\frac{\partial v}{\partial y}=0 \tag{1}$$

$$u\frac{\partial u}{\partial x}+v\frac{\partial u}{\partial y}=\frac{\mu_{nf}}{\rho_{nf}}\frac{\partial^2 u}{\partial y^2}-\frac{\sigma B_0^2}{\rho_{nf}}u-\frac{\mu_{nf}}{\rho_{nf}}\frac{1}{K_p}u \tag{2}$$

$$u\frac{\partial T}{\partial x}+v\frac{\partial T}{\partial y}=\alpha_{nf}\frac{\partial^2 T}{\partial y^2}-\frac{1}{(\rho C_p)_{nf}}\frac{\partial q_r}{\partial y} \tag{3}$$

where, u, v are the velocity components in the x and y directions respectively, ρ_{nf} is the density of the nanofluid, μ_{nf} is the dynamic viscosity of the nanofluid, T is the nanofluid temperature, q_r is the radiative heat flux, σ is the electrical conductivity of the nanofluid, $(\rho C_p)_{nf}$ is the heat capacitance of the nanofluid and α_{nf} its thermal diffusivity.

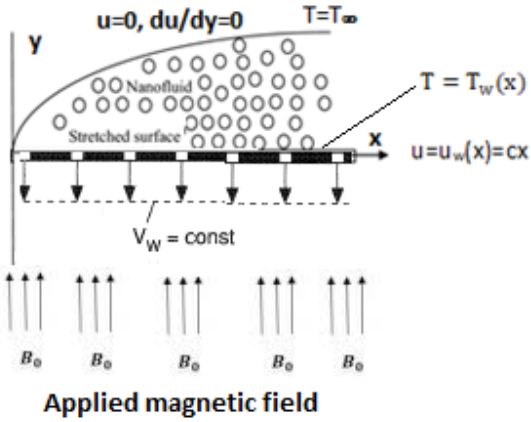

Figure 1. Flow configuration, boundary conditions and coordinate system

Using Rosseland approximation for radiation [16], we have:

$$q_r=-\frac{4\sigma^*}{3k^*}\frac{\partial T^4}{\partial y} \tag{4}$$

where, σ^* is the Stefan-Boltzmann constant, and k^* is the mean absorption coefficient.

Approximation (4) is valid at points optically far from the surface and it is good only for intensive absorption which is true for an optically thick boundary layer, such as the one considered in this paper.

By assuming that the temperature differences within the flow are sufficiently small, the term T^4 becomes a linear function of temperature. We can therefore expand it in a Taylor series about T_∞ and neglect higher order terms to get:

$$T^4 \approx 4T_\infty^3 T - 3T_\infty^4 \tag{5}$$

Therefore, Eq. (3) becomes:

$$u\frac{\partial T}{\partial x} + v\frac{\partial T}{\partial y} = \alpha_{nf}\frac{\partial^2 T}{\partial y^2} + \frac{16\sigma^* T_\infty^3}{3(\rho C_p)_{nf} k^*}\frac{\partial^2 T}{\partial y^2} = \left(\alpha_{nf} + \frac{16\sigma^* T_\infty^3}{3(\rho C_p)_{nf} k^*}\right)\frac{\partial^2 T}{\partial y^2} \tag{6}$$

The effective density, ρ_{nf}, thermal diffusivity α_{nf} and the heat capacitance $(\rho C_p)_{nf}$ of the nanofluid are given by:

$$\rho_{nf} = (1-\phi)\rho_f + \phi\rho_s \tag{7}$$

$$\alpha_{nf} = k_{nf}/(\rho C_p)_{nf} \tag{8}$$

$$(\rho C_p)_{nf} = (1-\phi)(\rho C_p)_f + \phi(\rho C_p)_s \tag{9}$$

where, ϕ is the nanoparticle volume fraction parameter and k_{nf} is the thermal conductivity of the nanofluid. Subscripts f and s refer to base fluid and nanoparticles, respectively.

The effective dynamics viscosity of the nanofluid was given by Brinkman [17]:

$$\mu_{nf} = \frac{\mu_f}{(1-\phi)^{2.5}} \tag{10}$$

And the thermal conductivity of the nanofluid restricted to spherical nanoparticles is approximated by the Maxwell-Garnett model [17]:

$$k_{nf} = k_f\left[\frac{(k_s + 2k_f) - 2\phi(k_f - k_s)}{(k_s + 2k_f) + \phi(k_f - k_s)}\right] \tag{11}$$

The values of the base fluid and the nanoparticles thermo-physical properties are given in Table 1.

Table 1. Thermo-physical properties of water and nanoparticles [16]

	ρ(kg/m^3)	C_p(J/kgK)	k(WmK)	B×10^5(K^{-1})
Pure water	997.1	4179	0.613	21
Copper (Cu)	8933	385	401	1.67
Copper oxide (CuO)	6320	531.8	76.5	1.80

The boundary conditions for Eqs. (1)-(3) are assumed in the form:

$$u = u_w(x) = u_0\left(\frac{x}{L}\right) = cx,\ v = v_w,\ T = T_w(x) = A\left(\frac{x}{L}\right)^2 + T_\infty \text{at } y = 0 \tag{12}$$

$$u \to 0, \frac{\partial u}{\partial y} \to 0,\ T \to T_\infty \text{ at } y \to \infty \tag{13}$$

where, A and c are constants, L is the characteristic length, T_∞ is the temperature of the fluid far from the sheet.

The continuity Eq. (1) is satisfied by introducing a stream function $\psi(x,y)$ such that:

$$u = \frac{\partial \psi}{\partial y},\ v = -\frac{\partial \psi}{\partial x} \tag{14}$$

The following similarity variables are also introduced [18]:

$$\eta = \frac{y}{\sqrt{K_p}},\ \psi = cx\sqrt{K_p}f(\eta), u = cxf'(\eta),\ v = -c\sqrt{K_p}f(\eta),\ \theta(\eta) = \frac{T - T_\infty}{T_w - T_\infty} \tag{15}$$

where, η is the similarity variable, ψ is the stream function, $f(\eta)$ is the non dimensionless stream function, $\theta(\eta)$ is the dimensionless temperature. By using Eqs. (6)-(9) and (13). Eqs. (2) and (5) are transformed into the following two-point boundary value problem:

$$f''' - (1-\phi)^{2.5}\left(1 - \phi + \phi\frac{\rho_s}{\rho_f}\right)\mathrm{DaRe}((f')^2 - ff'') - ((1-\phi)^{2.5}M_n\mathrm{DaRe} + 1)f' = 0 \tag{16}$$

$$\left(1 + \frac{4}{3}R\right)\theta'' - \frac{k_f}{k_{nf}}\left(1 - \phi + \phi\frac{\rho c_{p_s}}{\rho c_{p_f}}\right)\mathrm{PrDaRe}(2f'\theta - f\theta') = 0 \tag{17}$$

Which must satisfy the following boundary conditions.

$$f(0) = f_w,\ f'(0) = 1, f'(\infty) = \to 0 \tag{18}$$

$$\theta(0) = 1, \theta(\infty) \to 0 \tag{19}$$

where, $f_w = -Lv_w/u_0\sqrt{K_p}$ is the suction parameter.

The non-dimensional constants appearing in Eqs. (16)-(17) are the Darcy number Da, the Reynolds number Re, the magnetic parameter M_n, the radiation parameter R and the Prandtl number Pr, they are respectively defined as:

$$\mathrm{Da} = K_p/L^2;\mathrm{Re} = \frac{u_L L}{\nu_f};\ M_n = \frac{\sigma B_0^2}{c\rho_f};\mathrm{R} = 4\sigma^* T_\infty^3/k^*\, k_{nf} \text{ and } \mathrm{Pr} = \frac{\nu_f(\rho C_p)_f}{k_f} \tag{20}$$

In the present investigation, we define two important characteristics which are the local skin friction coefficient C_f and the local Nusselt number Nu_x [16]. These parameters characterize the surface drag and the wall heat transfer rate. The shear stress at the wall surface is given by:

$$\tau_w = -\mu_{nf}\left(\frac{\partial u}{\partial y}\right)_{y=0} \tag{21}$$

The local skin friction coefficient is defined by:

$$C_f = \frac{\tau_w}{\frac{1}{2}\rho_f u_w^2} = \frac{-2\mu_{nf}}{\rho_f u_w^2}\left(\frac{\partial u}{\partial y}\right)_{y=0} \tag{22}$$

Using Eqs. (9) and (14), the skin friction can be written as:

$$C_f \mathrm{Re}_x\sqrt{\mathrm{Da}_x} = -\frac{2}{(1-\phi)^{2.5}}f''(0) \tag{23}$$

where, $\mathrm{Re}_x = \frac{u_w x}{\nu_f}$ and $\mathrm{Da}_x = \frac{K_p}{x}$ is the local Reynolds and Darcy number.

The local Nusselt number Nu_x is defined as:

$$\mathrm{Nu_x} = \frac{\mathrm{x q_w}}{\mathrm{k_f(T_w - T_\infty)}} \tag{24}$$

where, q_w is the local heat flux at the wall and is given by:

$$\mathrm{q_w} = -\left(\mathrm{k_{nf}} + \frac{16\sigma^* \mathrm{T_\infty^3}}{3\mathrm{k}^*}\right)\left(\frac{\partial \mathrm{T}}{\partial \mathrm{y}}\right)_{\mathrm{y=0}} \tag{25}$$

Using Eq. (25) in Eq. (24), the local Nusselt number can be expressed as:

$$\mathrm{Nu_x}\sqrt{\mathrm{Da_x}} = \frac{-\mathrm{k_{nf}}}{\mathrm{k_f}}\left(1 + \frac{4}{3}\mathrm{R}\right)\theta'(0) \tag{26}$$

3. NUMERICAL METHOD FOR SOLUTION

In this investigation, we used the fourth order Rung-Kutta - Fehlberg method in conjunction with the shooting technique [19] to solve the non linear coupled differential equations Eqs. (16) and (17) along with the boundary conditions (18-19). The third order differential Eq. (16) is replaced by three first order equations while the second order Eq. (17) is replaced by two first order equations. Let $y_1=f$, $y_2=f'$, $y_3=$f'' and $y_4=\theta$. We get the following system of five first order differential equations for a simultaneous solution.

$$y_1' = y_2 \tag{27}$$

$$y_2' = y_3 \tag{28}$$

$$y_3' = (1-\phi)^{2.5}\left[1 - \phi + \phi\frac{\rho_s}{\rho_f}\right]\mathrm{DaRe}\,[(y_2)^2 - y_1 y_3)] - ((1-\phi)^{2.5}\mathrm{M_n DaRe} + 1)y_2 \tag{29}$$

$$y_4' = y_5 \tag{30}$$

$$y_5' = \frac{1}{(1+\frac{4}{3}\mathrm{R})}\frac{\mathrm{k_f}}{\mathrm{k_{nf}}}\left(1 - \phi + \phi\frac{\rho c_{p_s}}{\rho c_{p_f}}\right)\mathrm{PrDaRe}(2y_2\, y_4 - y_1\, y_5) \tag{31}$$

With the boundary conditions:

$$y_1(0) = f_w,\ y_2(0) = 1 \text{ and } y_4(0) = 1 \tag{32}$$

$$y_2(\infty) \to 0 \text{ and } y_4(\infty) \to 0 \tag{33}$$

The numerical procedure is carried out by guessing the values of $f''(0)$(ie $y_3(0)$)and $\theta'(0)$(ie $y_5(0)$)which are then improved until the end boundary conditions are satisfied. The computations were stopped when the relative error (convergence criterion) between the newly calculated and previously calculated variables' values reaches the value 10^{-8}.

4. RESULTS AND DISCUSSION

In this paper, the steady two-dimensional laminar MHD flow and heat transfer of a nanofluid through a porous medium with radiation effect over a stretching sheet is investigated. The results are presented in Figures 2-23 and in Table 2. They show the effects of nanoparticles volume fraction, Darcy and Reynolds numbers, magnetic, suction and radiation parameters on velocity, temperature profiles, the coefficient of skin friction and the Nusselt number for the two nanofluids Cu-water and CuO-water.

4.1 Effect of nanoparticle volume fraction on velocity and temperature profiles

Figures 2 and 3 depict the influence nanoparticle volume fraction on both longitudinal and transverse velocity profiles for two values of the magnetic field (M_n=0.03, M_n=3.0). It is observed that for a small value of the magnetic field (M_n=0.03), the velocity profiles decrease with increasing values of nanoparticle volume fraction, physically, this means that the adding of the solid particles in the base fluid causes an increase of the dynamics viscosity and momentum diffusion of the fluid, thus, the thickness of the boundary layer decreases. While the opposite behavior happens with the velocity for high value of magnetic field (M_n=3) as can be noted in Figure 3, the velocity increases with increasing values of ϕ. Also, a comparison of the profiles for a given value of ϕ (for example ϕ=0.2) shows that an increase of the magnetic field slows down the flow motion. Figure 4 shows the temperature profile for different values of nanoparticle volume fraction and magnetic parameter. It can be seen that the temperature increases with the increasing in the volume fraction of the nanoparticles. The presence of solid nanoparticles in the base fluid increases the thickness of the thermal boundary layer.

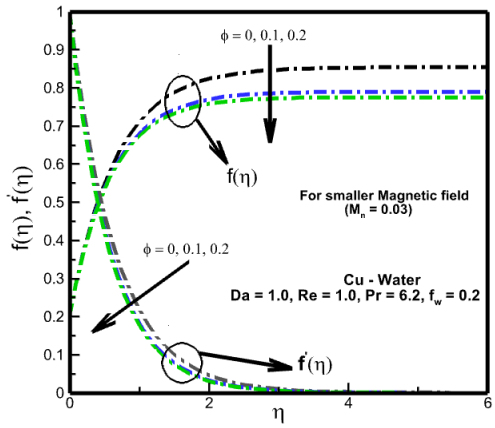

Figure 2. Effects of nanoparticles volume fraction on dimensionless velocity

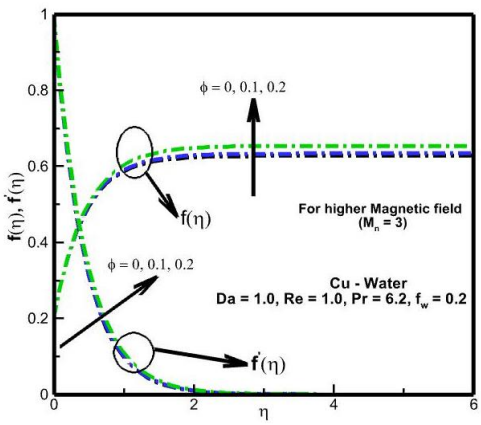

Figure 3. Effects of nanoparticles volume fraction on dimensionless velocity

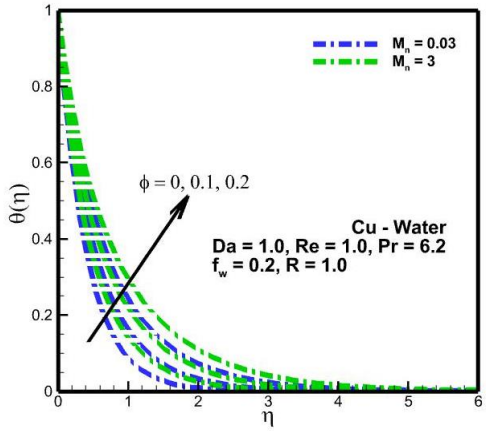

Figure 4. Influence of nanoparticles volume fraction and magnetic parameter on dimensionless temperature

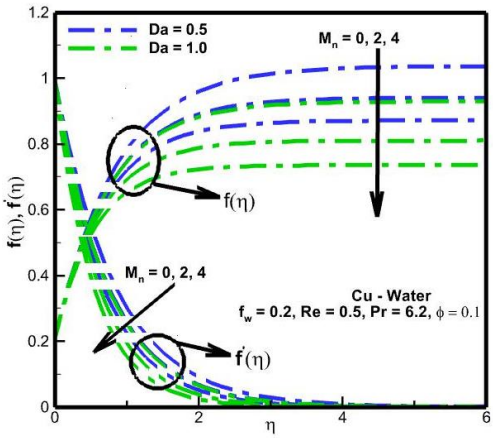

Figure 5. Influence of M_n and Da on dimensionless velocity

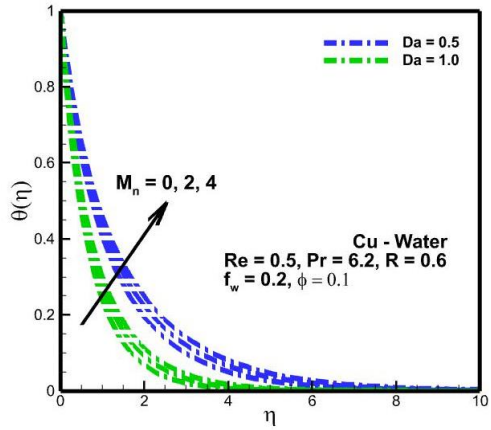

Figure 6. Influence of M_n and Da on dimensionless temperature

4.2 Effect of the magnetic field on velocity and temperature profiles

The effect of the magnetic parameter on velocity and temperature profile of Cu-water is shown in Figures 5 and 6. It is noted that the increasing values of the magnetic parameter decrease the velocity profiles. Due to Lorentz force which produces resistance to flow, the hydrodynamics boundary layer decreases with the magnetic parameter. However, Figure 6 shows that an increase in the magnetic parameter results in an increase of the temperature. The presence of the magnetic parameter decelerates the flow and leads to an increase in friction, thus, the fluid temperature is enhanced with an increase in Mn.

4.3 Effect of the Darcy number Da on velocity and temperature profiles

Figures 7 and 8 illustrate the effect of Daon velocity and temperature profiles of the nanofluid in the case of Cu-Water when *Pr*=6.2. It is observed that the increase of Da leads to a decrease of both the velocity and the temperature of the nanofluid. The presence of the porous medium causes higher restriction to the fluid, thus, the thickness of the thermal and hydrodynamics boundary layer decreases.

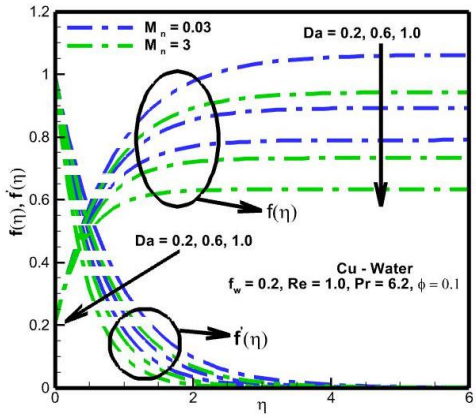

Figure 7. Influence of M_n and Da on dimensionless velocity

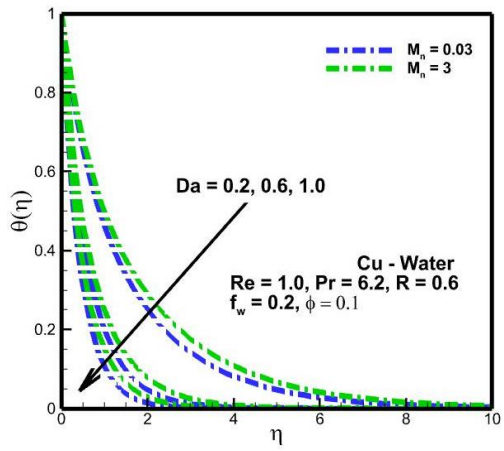

Figure 8. Influence of M_n and Da on dimensionless temperature

4.4 Effect of Reynolds number and magnetic parameter on velocity and temperature profiles

Figures 9 and 10 show the influences of Reynolds number and magnetic parameter on velocity and temperature profiles. It can be seen that an increase in Reynolds number Re causes the velocity and the temperature of the fluid to decrease; this can be explained as follows: as the Reynolds number is increased the viscous forces become less important, and therefore the momentum transfer between fluid layers diminishes thus leading to low velocity profiles, which in turn diminish the heat transfer between fluid layers and therefore lead to low temperatures within the fluid.

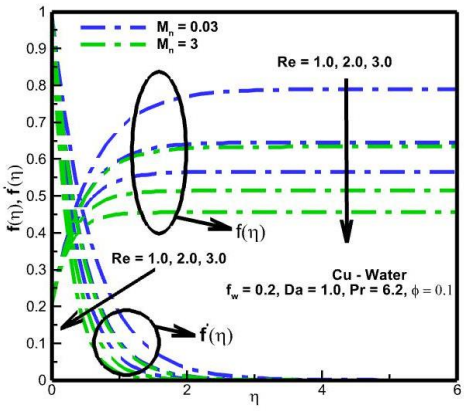

Figure 9. Influence of Re and M_n on dimensionless velocity

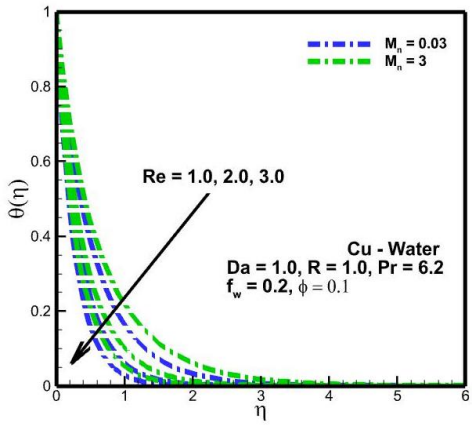

Figure 10. Influence of Re and M_n on dimensionless temperature

4.5 Effect of suction and magnetic parameters on velocity and temperature profiles

Figures 11 and 12 show the influence of suction and magnetic parameters on velocity and temperature profiles. It can be seen that an increase in suction parameter f_w causes the velocity and the temperature of the fluid to decrease.

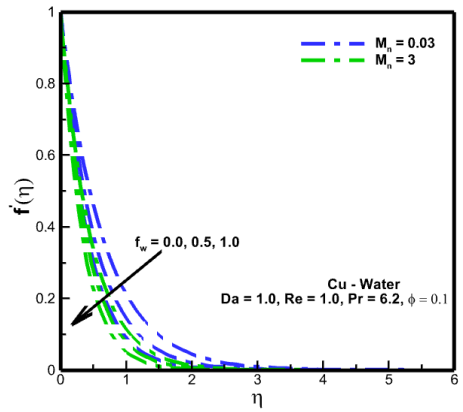

Figure 11. Influence of f_w parameter and M_n on dimensionless velocity

4.6 Effect of nanoparticle type on velocity and temperature profiles

Figures 13 and 14 show the effect of two types of solid nanoparticles (Copper and Copper oxide) on dimensional velocity and temperature. It is obvious from Figure 13 that the velocity of the CuO-water nanofluid is greater than that of the Cu-water nanofluid. However, Figure 14 shows that the Copper nanofluid increases the temperature compared to that of the Copper oxide nanofluid. This is due to the fact that Copper has a significantly higher conductivity than Copper oxide and therefore, the thickness of the thermal boundary layer of the Copper nanofluid is larger than that of the Copper oxide nanofluid.

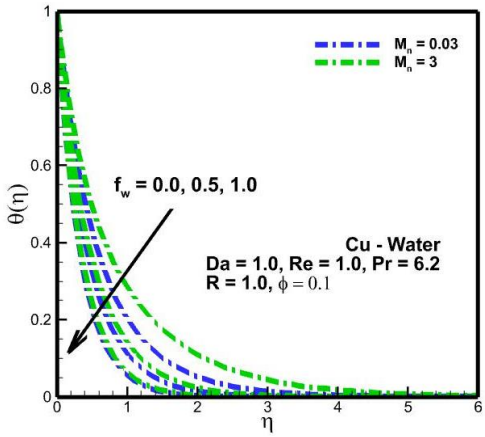

Figure 12. Influence of f_w and M_n on dimensionless temperature

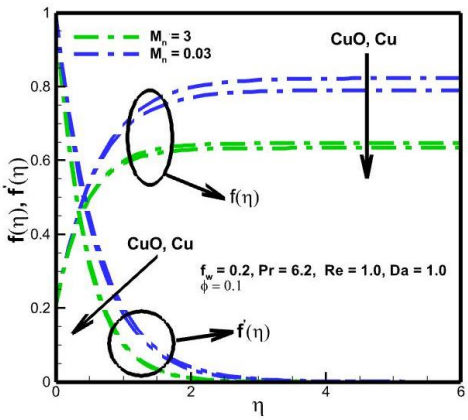

Figure 13. Influence of M_n on velocity profiles for CuO and Cu nanofluids

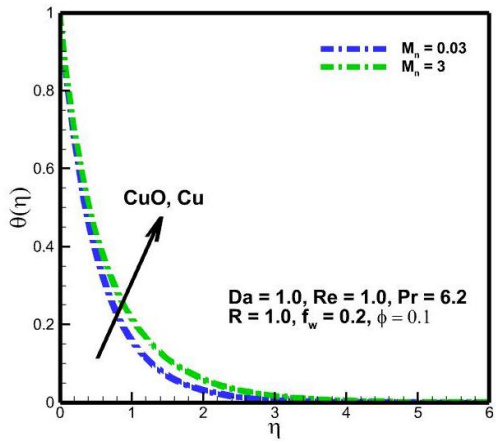

Figure 14. Influence of M_n on temperature profiles for CuO and Cu nanofluids

4.7 Effect of radiation parameter R and magnetic parameter on temperature profiles

Figure 15 is presented to show the influence of radiation

parameter R and magnetic parameter on temperature variation within the Cu-water nanofluid. It can be seen that the temperature profile decreases with increasing in the parameter of the thermal radiation R, this is due to an increase in the heat transfer coefficient between the nanofluid and stretching surface.

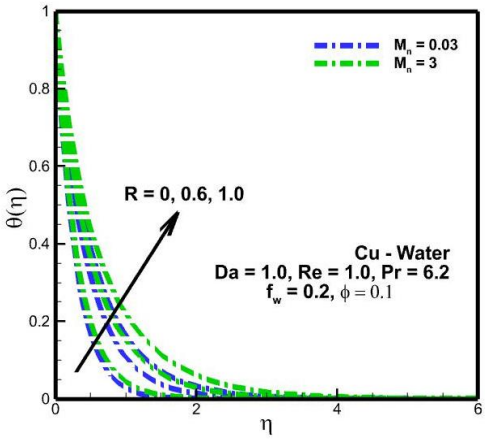

Figure 15. Influence of R and M_n on dimensionless temperature

4.8 Effect of M_n, Da, f_w, R and ϕ on the local friction coefficient and the Nusselt number

Figures 16-24 depict the effect of M_n, Da, f_w, R and the nanoparticles volume fraction ϕ on the coefficient of the local friction and Nusselt number for Copper and Copper oxide water based nanofluids. From these figures, we can observe that the skin-friction coefficient and local Nusselt number both increase with the increase in the value of ϕ. Furthermore, it is obvious that the effect of adding nanoparticles to the base fluid affects considerably the values of C_f and Nu. The values of C_f and Nu become higher when Da and Re are increased. The value of the local friction and Nusselt number for Copper and Copper oxide nanofluids are computed and tabulated in Table 2. The computations for M_n=1, 2 and 3 were carried out while the values of the remaining parameters are kept constant: ϕ=0.1, Da=0.6, Re=2, f_w=0.2 and R=2. The computations for ϕ=0.05, 0.10 and 0.15 were carried out while the values of the remaining parameters are kept constant: M_n=2, Da=0.6, Re=2, f_w=0.2 and R=2. The computations for Da=0.2, 0.6 and 1.0 were carried out while the values of the remaining parameters are kept constant: ϕ=0.1, M_n=2, Re=2, f_w=0.2 and R=2. The computations for Re=1, 2 and 3 were carried out while the values of the remaining parameters are kept constant: ϕ=0.1, Da=0.6, M_n=2, f_w=0.2 and R=2. The computations for R=1, 2 and 3 were carried out while the values of the remaining parameters are kept constant: ϕ=0.1, Da=0.6, M_n=2, f_w=0.2 and Re=2. It can be noticed from the table that the coefficient of local friction increases with the increasing values of M_n, Da, Re and f_w. The Nusselt number increases with ϕ, Da, f_w and R, but decreases with M_n. A comparison of the Cu and the CuO nanofluids results shows that the coefficient of friction of Copper oxide nanofluids is smaller than that of Copper while the Nusselt number values of Copper oxide are greater than those of the Copper nanofluid.

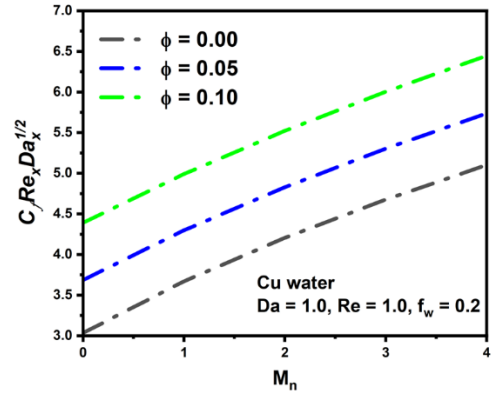

Figure 16. Influence of ϕ and M_n on skin friction coefficient

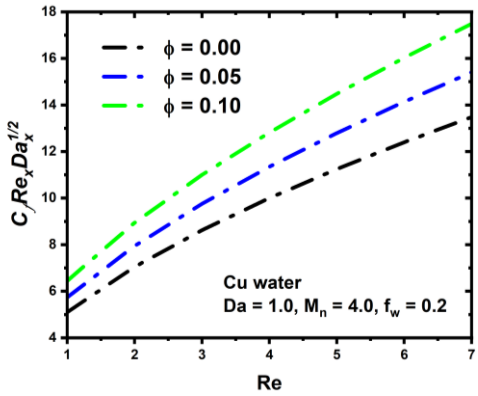

Figure 17. Influence of ϕ and Re on skin friction coefficient

Table 2. Values of $C_f Re_x \sqrt{Da_x}$ and $Nu_x \sqrt{Da_x}$ for various values of governing parameters

		$C_f Re_x \sqrt{Da_x}$		$Nu_x \sqrt{Da_x}$	
		Cu	**CuO**	**Cu**	**CuO**
	1	5.3731118	5.1364650	7.7878978	7.8766873
M_n	2	5.9691371	5.7517610	7.5146021	7.5918082
	3	6.5069734	6.3036120	7.2776906	7.3460391
	0.05	5.2164572	5.1091162	7.2926750	7.3313904
ϕ	0.10	5.9691371	5.7517610	7.5146021	7.5918082
	0.15	6.8124647	6.4811493	7.7504593	7.8646104
	0.2	3.9775128	3.8839704	3.8467868	3.8773842
Da	0.6	5.9691371	5.7517610	7.5146021	7.5918082
	1.0	7.5600239	7.2422991	10.1591320	10.271298
	1	4.5370780	4.4083863	4.9554814	4.9998391
Re	2	5.9691371	5.7517610	7.5146021	7.5918082
	3	7.1855216	6.8917388	9.5467896	9.6507796
	1			6.6451779	6.6909807
R	2			7.5146021	7.5918082
	3			8.0876296	8.1918702

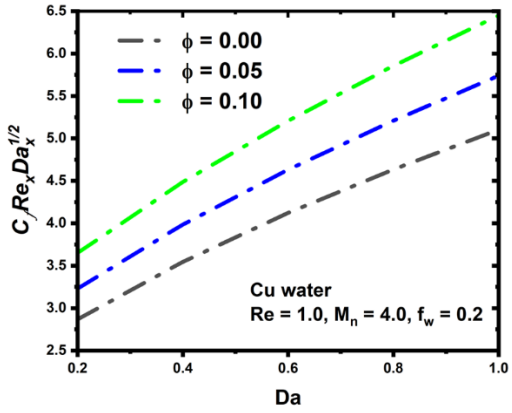

Figure 18. Influence of ϕ and Da on skin friction coefficient

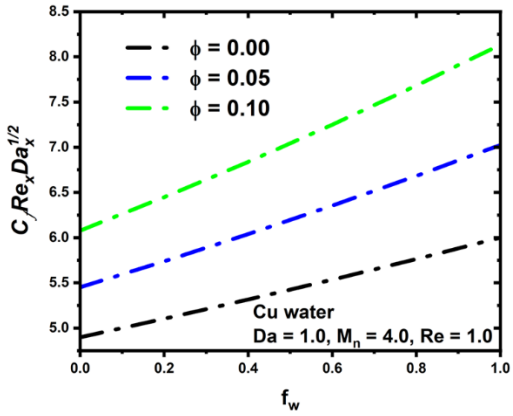

Figure 19. Influence of ϕ and f_w on skin friction coefficient

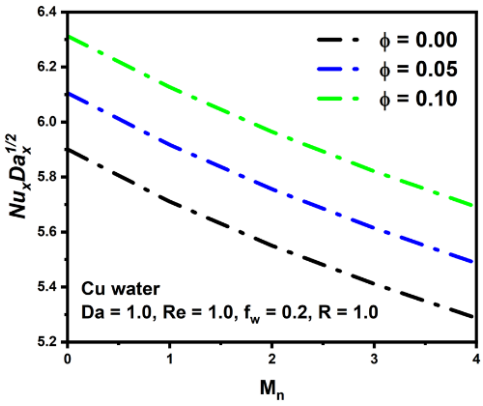

Figure 20. Influence of ϕ and M_n on dimensionless heat transfer

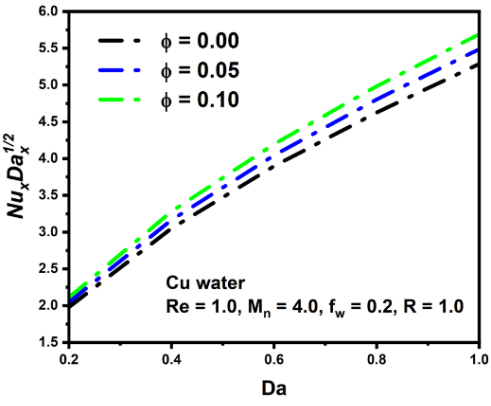

Figure 21. Influence of ϕ and Da on dimensionless heat transfer

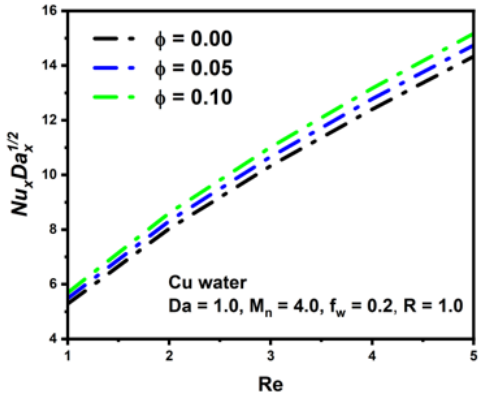

Figure 22. Influence of ϕ and Re on dimensionless heat transfer

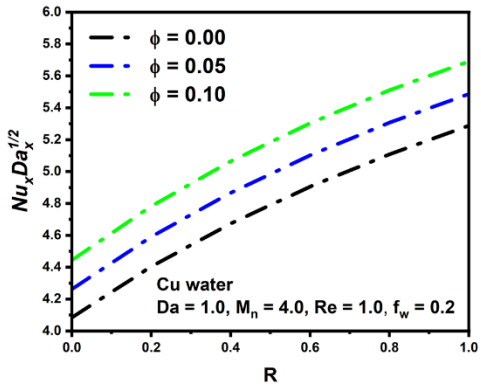

Figure 23. Influence of ϕ and R on dimensionless heat transfer

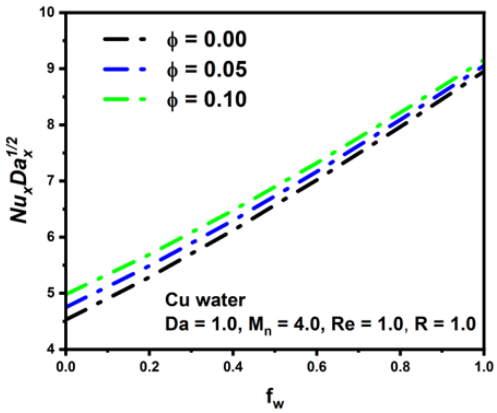

Figure 24. Influence of ϕ and f_w on dimensionless heat transfer

5. CONCLUSION

In this paper, the steady two dimensional, incompressible water based MHD nanofluid flow over a stretching sheet through porous medium with radiation effects is investigated. Both Cu-water and CuO-water nanofluids flows were simulated. The results obtained have been presented in a graphical or tabular form and showed the influence of nanoparticle volume fraction, magnetic field, Darcy number, Reynolds number, suction parameter and radiation conductivity parameter on the velocity and temperature fields as well as the heat transfer and friction characteristics. To realize these objectives, the partial differential equations

governing the laminar flow were first transformed into nonlinear ordinary differential equations using similarity variables. The resulting ODE's, which constitute a boundary value problem, were then solved numerically using the fourth order Runge-Kutta method with the shooting technique.

The following conclusions can be drawn from the analysis of the results:

-An increase in M_n, Da, Re and f_w tends to reduce the velocity of the nanofluids.

-An increase in ϕ, Mn and R leads to a rise of the temperature profiles. The opposite effect takes place when the parameters Da, Re and f_w are increased.

-The adding of the solid particles in the base fluid causes an increase of the dynamics viscosity and momentum diffusion of the fluid, thus, the thickness of the boundary layer decreases.

-Due to Lorentz force which produces resistance to flow, the hydrodynamics boundary layer decreases with the magnetic parameter.

-The presence of the magnetic parameter decelerates the flow and leads to an increase in friction, while the fluid temperature is enhanced with an increase in M_n.

-The presence of the porous medium causes higher restriction to the fluid, thus, the thickness of the thermal and hydrodynamics boundary layers decrease.

-As the Reynolds number is increased the viscous forces become less important, and therefore the momentum transfer between fluid layers diminishes thus leading to low velocity profiles, which in turn diminish the heat transfer between the fluid layers and therefore lead to low temperatures within the fluid.

-The Copper has a higher conductivity than Copper oxide and therefore, the thickness of the thermal boundary layer of the Copper nanofluid is larger than that of the Copper oxide nanofluid.

-The skin-friction coefficient and local Nusselt number both increase with the increase in the value of ϕ.

-The values of C_f and Nu become higher when Da and Re are increased.

-The coefficient of local friction increases with M_n, Da, Re and f_w.

-The Nusselt number increases with ϕ, Da, f_w and R but decreases with M_n.

-A comparison of the Cu and the CuO nanofluids results shows that the coefficient of friction of copper oxide nanofluids is smaller than that of Copper while the Nusselt number values of Copper oxide are greater than those of the Copper nanofluid. Therefore, to achieve a maximum heat transfer rate and minimum skin friction coefficient, it is better to use Copper oxide nanoparticles.

These study's findings can be exploited partially or totally in the design and optimization of the following manufacturing processes: Wire drawing, paper production, glass-fiber production, hot metal rolling, metal and polymer extrusion processes as well as drawing of plastic films and metal spinning.

Finally the following limitations of the present study are acknowledged by the authors: the type of nanofluid, the approximation of the radiation flux, the flow regime, the types of transfers involved, the dimensionality of the flow over the stretching sheet, the numerical method and the boundary conditions. The authors suggest for future work to address these limitations by investigating other types of nanofluids, by improving the approximation of the radiation flux, by studying the turbulent flow, by including mass transfer of species which may be created due to chemical reactions on the sheet surface, by studying the three dimensional flow and by using other more accurate numerical methods such as the finite difference method, the finite volume method or the finite element method. The study could also be conducted with more realistic boundary conditions specific to the various manufacturing processes.

REFERENCES

[1] Mandal, I.C., Mukhopadhyay, S. (2013). Heat transfer analysis for fluid flow over an exponentially stretching porous sheet with surface heat flux in porous medium. Ain Shams Engineering Journal, 4(1): 103-110. https://doi.org/10.1016/j.asej.2012.06.004

[2] Das, S.K., Choi, S.U.S., Yu, W., Pradeep, T. (2007). Nanofluids: Science and Technology. Wiley, New York. https://www.academia.edu/7423331/NANOFLUIDS_NANOFLUIDS_Science_and_Technology.

[3] Das, K. (2015). Nanofluid flow over a non-linear permeable stretching sheet with partial slip. Journal of the Egyptian Mathematical Society, 23(2): 451-456. https://doi.org/10.1016/j.joems.2014.06.014

[4] Balla, C.S., Kishan, N., Gorla, R.S.R., Gireesha, B.J. (2017). MHD boundary layer flow and heat transfer in an inclined porous square cavity filled with nanofluids, Ain Shams Engineering Journal, 8(2): 237-254. https://doi.org/10.1016/j.asej.2016.02.010

[5] Abdollahi, A., Mohammed, H.A., Vanaki, S.M., Sharma, R.N. (2018). Numerical investigation of fluid flow and heat transfer of nanofluids in microchannel with longitudinal fins. Ain Shams Engineering Journal, 9(4): 3411-3418. https://doi.org/10.1016/j.asej.2017.05.011

[6] Aghaei, A., Sheikhzadeh, G.A., Dastmalchi, M., Forozande, H. (2015). Numerical investigation of turbulent forced-convective heat transfer of Al_2O_3–water nanofluid with variable properties in tube. Ain Shams Engineering Journal, 6(2): 577-585. https://doi.org/10.1016/j.asej.2014.11.015

[7] Gundabattini, E., Kuppan, R., Solomon, D.G., Kalam, A., Kothari, D.P., Bakar, R.A. (2021). Review on methods of finding losses and cooling methods to increase efficiency of electric machines. Ain Shams Engineering Journal, 12(1): 497-505. https://doi.org/10.1016/j.asej.2020.08.014

[8] Ho, C.J., Chang, C.Y., Yan, W.M., Amani, P. (2018). A combined numerical and experimental study on the forced convection of Al_2O_3-water nanofluid in a circular tube. International Journal of Heat and Mass Transfer, 120: 66-75. https://doi.org/10.1016/j.ijheatmasstransfer.2017.12.031

[9] Zubair, M.M., Seraj, M., Faizan, M., Anas, M., Yahya, S.M. (2021). Experimental study on heat transfer of an engine radiator with TiO_2/EG-water nano-coolant. SN Applied Sciences, 3: 434. https://doi.org/10.1007/s42452-021-04441-7

[10] Crane, L.J. (1970). Flow past a stretching plate. Journal of Applied Mathematics and Physics, 21: 645-655. http://doi.org/10.1007/BF01587695

[11] Carragher, P., Crane, L.J. (1982). Heat transfer on a continuous stretching sheet. Journal of Applied Mathematics and Mechanics, 62: 564-573. http://doi.org/10.1002/zamm.19820621009

[12] Magyari, E., Keller, B. (1999). Heat and mass transfer in the boundary layers on an exponentially stretching continuous surface. Journal of Physics D, 32(5): 577-585. http://doi.org/10.1088/0022-3727/32/5/012

[13] Sajid, M., Hayat, T. (2008). Influence of thermal radiation on the boundary layer flow due to an exponentially stretching sheet. International Communications in Heat and Mass Transfer, 35(3): 347-356. http://doi.org/10.1016/j.icheatmasstransfer.2007.08.006

[14] Ramya, D., Srinivasa Raju, R., Anand Rao, J., Rashidi, M.M. (2016). Boundary layer viscous flow of nanofluids and heat transfer over a nonlinearly isothermal stretching sheet in the presence of heat generation/absorption and slip boundary conditions. International Journal of Nanoscience and Nanotechnology, 12: 251.

[15] Ahmed, S., Pop, I. (2010). Mixed convection boundary layer flow from a vertical flat plate embedded in a porous medium filled with nanofluids. International Communications in Heat and Mass Transfer, 37: 987-991. http://doi.org/10.1016/j.icheatmasstransfer.2010.06.004

[16] Rashidi, M.M., Vishnu Ganesh, N., Abdul Hakeem, A.K., Ganga, B. (2014). Buoyancy effect on MHD flow of nanofluid over a stretching sheet in the presence of thermal radiation. Journal of Molecular Liquids, 198: 234-2384. https://doi.org/10.1016/j.molliq.2014.06.037

[17] Brinkman, H.C. (1952). The viscosity of concentrated suspensions and solutions. The Journal of Chemical Physics, 20(4): 571-581. https://doi.org/10.1063/1.1700493

[18] Mabood, F., Khan, W.A. (2014). Homotopy analysis method for boundary layer flow and heat transfer over a permeable flat plate in a Darcian porous medium with radiation effects. Journal of the Taiwan Institute of Chemical Engineers, 45(4): 1217-1224. http://doi.org/10.1016/j.jtice.2014.03.019

[19] Gerald, C.F., Wheatly, P.O. (2004). Applied Numerical Analysis, Seventh Edition. Pearson Addison Wesley Publishers. https://www.cse.iitm.ac.in/~vplab/downloads/opt/Applied%20Numerical%20Analysis.pdf.

NOMENCLATURE

B_0	magnetic flux density, T(Tesla)
C_{fx}	local skin friction coefficient
C_p	specific heat at constant pressure, J. kg^{-1}. K^{-1}
Da	Darcy number
Da_x	local Darcy number
$f(\eta)$	dimensionless stream function
f_w	suction parameter
k^*	mean absorption coefficient, m^{-1}
k_f	thermal conductivity of the base fluid, $W.m^{-1}.K^{-1}$
k_s	thermal conductivity of nanoparticles, $W.m^{-1}.K^{-1}$
k_{nf}	thermal conductivity of the nanofluid, $W.m^{-1}.K^{-1}$
K_p	porous medium permeability, m^2
L	characteristic length, m
Mn	magnetic parameter
Nu_x	local Nusselt number
Pr	Prandtl number
q_r	radiative heat flux in the y direction, $W.m^{-2}$
q_w	heat flux at the wall, $W.m^{-2}$
R	radiation parameter
Re	Reynolds number
Re_x	local Reynolds number
T	fluid temperature, K
T_w	temperature at the surface of the sheet, K
$T\infty$	fluid temperature far from the stretching sheet, K
u	velocity component in the x-direction, $m.s^{-1}$
u_0	wall velocity coefficient, $m.s^{-1}$
u_w	velocity of the wall along the x-axes, $m.s^{-1}$
v	velocity component in the y-direction, $m.s^{-1}$
v_w	suction velocity, $m.s^{-1}$
x	coordinate parallel to the sheet, m
y	coordinate normal to the sheet, m

Greek symbols

α_{nf}	thermal diffusivity, $m^2.s^{-1}$
η	dimensionless similarity variable.
Θ	dimensionless temperature
μ	dynamic viscosity, kg. $m^{-1}.s^{-1}$
ν	kinematic viscosity, $m^2.s^{-1}$
ρ	density, kg. m^{-3}
σ	electrical conductivity of the nanofluid, $S.m^{-1}$(Siemens per meter)
σ^*	Stefan-Boltzmann constant, $\sigma^*=5.67.10^{-8}$ $W.m^{-2}.K^4$
τ_w	shear stress at the wall, $N.m^{-2}$
ϕ	solid volume fraction
ψ	stream function, $m^2.s^{-1}$

Subscripts

s	nanoparticle
f	fluid (pure water)
nf	nanofluid